ELSEVIER

Journal of Organometallic Chemistry 493 (1995) 153–162

Journal of Organometallic Chemistry

Synthesis and spectroscopic properties of Re(R)(CO)$_3$(α-diimine) (R = alkyl; α-diimine = R′-pyCa, R′-DAB) complexes. Crystal structure of Re(Me)(CO)$_3$(^{i}Pr-DAB)

Brenda D. Rossenaar [a], Cornelis J. Kleverlaan [a], Maartje C.E. van de Ven [a], Derk J. Stufkens [a,*], Ad Oskam [a], Jan Fraanje [b], Kees Goubitz [b]

[a] *Anorganisch Chemisch Laboratorium, J.H. van 't Hoff Research Institute, Universiteit van Amsterdam, Nieuwe Achtergracht 166, 1018 WV Amsterdam, The Netherlands*

[b] *Laboratorium voor Kristallografie, Amsterdam Institute for Molecular Studies, Universiteit van Amsterdam, Nieuwe Achtergracht 166, 1018 WV Amsterdam, The Netherlands*

Received 10 October 1994

Abstract

The synthesis, structure and spectroscopic properties of several complexes of the type Re(R)(CO)$_3$(α-diimine) (R = alkyl) are reported. The structure of Re(Me)(CO)$_3$(^{i}Pr-DAB) has been determined by a single-crystal X-ray diffraction study. The molecule has a distorted octahedral geometry, with the three carbonyls in a *fac*-geometry. The complexes possess strong absorption bands in the visible region which are assigned to MLCT transitions with the aid of resonance Raman spectroscopy; the Raman spectra do not provide any evidence for a σ(Re — R) → π^*(α-diimine) transition within this absorption band. The UV-vis spectrum of Re(Bz)(CO)$_3$(^{i}Pr-DAB) (Bz = benzyl) shows a distinct shoulder at the low-energy side of the visible band, which is attributed to the interaction between the dπ(Re)-orbitals and the π-orbitals of the benzyl group. The UV–photoelectron spectrum of Re(Me)(CO)$_3$(^{i}Pr-DAB) shows that σ(Re — Me) has a higher ionization potential than the dπ(Re)-orbitals, a result that is of importance for the interpretation of the photochemical behaviour of this complex.

Keywords: Raman spectroscopy; Crystal structure; Rhenium; Photoelectron spectroscopy; Diimine; Alkyl

1. Introduction

Metal–metal-bonded complexes of the type L_nM — Re(CO)$_3$(α-diimine) (L_nM = (CO)$_5$Mn, (CO)$_5$Re, (CO)$_4$Co, Cp(CO)$_2$Fe, Ph$_3$Sn, etc.) undergo efficient homolysis of the M — Re bond upon irradiation into their lowest-energy absorption band [1–5]. This was rather unexpected, since visible excitation leads to occupation of a non-reactive MLCT state. It has therefore been assumed that this reaction does not proceed from an MLCT state but from a close-lying reactive state [6]. In view of the high quantum yields, surface crossing to this state has to be fast.

The reactive quenching of the MLCT states of these complexes seems to be related to the behaviour of the chromophore-quencher (C-Q) complexes Re(D)(CO)$_3$-(α-diimine)$^+$ (D = organic electron donor) [7–9], the emission of which is quenched by intramolecular electron transfer from D to Re^{II} in the ^{3}MLCT state. For the metal–metal-bonded complexes, a similar intramolecular electron transfer in the ^{3}MLCT state might occur from the metal–metal bonding orbital (σ) to Re^{II}. The complex then arrives in a $^3\sigma\pi^*$ state.

For the complexes R$_2$Zn(α-diimine) (R = alkyl), occupation of this $^3\sigma\pi^*$ state leads to homolysis of a Zn–alkyl bond [10]. By analogy, the homolysis reactions of the metal–metal-bonded complexes have been explained in terms of a similar reaction from the $^3\sigma\pi^*$ state of these complexes [6]. In contrast to the R$_2$Zn(α-diimine) complexes, the metal–metal-bonded complexes do not possess an intense $\sigma \rightarrow \pi^*$ transition and the reactive $^3\sigma\pi^*$ state can only be occupied by surface crossing from an MLCT state.

* Corresponding author.

SSDI 0022-328X(95)05392-1

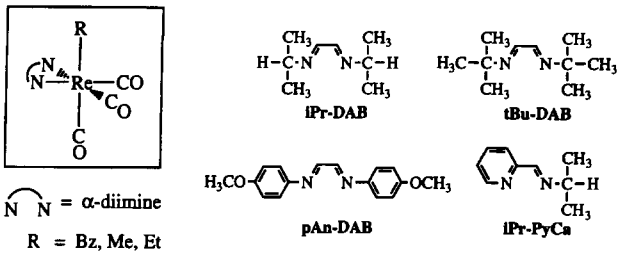

Fig. 1. Schematic structures of the complexes Re(R)(CO)$_3$(α-diimine) and the ligands used.

For the metal–metal-bonded complexes, the quantum yields of the homolysis appeared to be high and temperature-independent, which means that the reactive $^3\sigma\pi^*$ state is lower in energy than the MLCT states. This conclusion was confirmed by the UV–photoelectron spectra of these complexes which showed the σ-orbitals to have a lower ionization energy (IE) than the dπ(Re) orbitals [11].

In order to investigate whether the efficiency of the homolysis reaction can be influenced by variation of the relative IEs of the σ- and dπ-orbitals, we have synthesized the two series of complexes Ru(X)(R)(CO)$_2$(α-diimine) (X = halide; R = alkyl) and Re(R)(CO)$_3$(α-diimine) (R = alkyl). The spectroscopic, photophysical and photochemical properties of the first set of complexes have been described elsewhere [12–14], while the synthesis, structural and spectroscopic properties of the second set are reported here. A preliminary account of the photochemistry of these Re complexes has appeared [15]. The general structure of the complexes is shown in Fig. 1.

2. Experimental details

2.1. Materials

$Re_2(CO)_{10}$ (Strem), Br_2, MeMgCl, EtBr (Merck), BzCl (EGA-Chemie) and MeI (Aldrich) were obtained commercially and used without further purification. Silica gel for column chromatography (Kieselgel 60, 70–230 mesh, Merck) was activated by heating overnight in vacuo at 160°C.

Solvents for synthetic purposes were of reagent grade and carefully dried over sodium wire (THF, n-hexane, diethyl ether), $CaCl_2(CH_2Cl_2)$ or P_2O_5 (CH_3CN) and freshly distilled under nitrogen prior to use. Solvents for spectroscopy were of analytical grade, dried over sodium and distilled under N_2 before use.

The ligands *N,N'*-diisopropyl-1,4-diaza-1,3-butadiene (^{i}Pr-DAB), *N,N'*-di-t-butyl-1,4-diaza-1,3-butadiene (^{t}Bu-DAB), *N,N'*-di-*p*-anisyl-1,4-diaza-1,3-butadiene (*p*An-DAB) and pyridine-2-carbaldehyde-*N*-isopropylimine (^{i}Pr-pyCa) [16], and EtMgBr, were synthesized by published procedures.

2.2. Preparation of the complexes

All complexes were prepared under nitrogen using standard inert gas techniques. At all stages light was excluded to prevent photochemical decomposition.

The complexes Re(R)(CO)$_3$(R'-DAB) (R,R' = Me, ^{i}Pr; Et, ^{i}Pr; Bz, ^{i}Pr; Me, ^{t}Bu; Et, ^{t}Bu; Bz, ^{t}Bu; Me, *p*An) were all prepared by a modified procedure based on that described by García Alonso et al. [17]. To a solution of 0.5 mmol Re(Br)(CO)$_3$(R'-DAB) [18] in 50 ml of THF was added an excess of $Na_{2.8}$ K alloy. This mixture was stirred until conversion to the reduced complex was complete (ca. 2 h). Excess NaK was filtered off. The solution was cooled in an ice/salt/water bath to −20°C and 0.5 ml of the appropriate alkyl halide (MeI, EtBr or BzCl) was added. The desired complex was formed at once as shown by the immediate colour change. Evaporation of the solvent in vacuo left the complex Re(R)(CO)$_3$(R'-DAB) which was purified by column chromatography on silica using n-hexane/THF. Yield, 30%–50%.

For the complexes Re(R)(CO)$_3$(^{i}Pr-pyCa) (R = Me, Et) a different route had to be used because of the instability of the reduction product of Re(Br)(CO)$_3$(^{i}Pr-pyCa). Thus, 0.5 mmol of Re(Br)(CO)$_3$(^{i}Pr-pyCa), made by stirring a THF solution of Re(Br)(CO)$_3$(CH_3CN)$_2$ with a slight excess of ^{i}Pr-pyCa for 1 h, was dissolved in 15 ml of THF. To this solution, cooled in a Dry Ice/ethanol bath to −80°C, was added an excess of the relevant Grignard reagent (0.3 ml of 0.3 M MeMgCl in THF or 0.8 ml of 0.1 M EtMgBr in diethyl ether). The product was formed immediately. The cooled solution was created with 0.1 ml of CH_2Cl_2 to stop the reaction. The magnesium salts were removed from the mixture by flash column chromatography of the solution on a short silica column. After evaporation of the solvent, the complex was purified by column chromatography on silica using gradient elution with n-hexane THF. Yield, 50%–80%.

^{i}Pr-DAB: ^{1}H NMR ($CDCl_3$)δ: 7.92 (2H, s, N=C*H*); 3.51 (2H, sept, *J* = 6.3 Hz, C*H*(CH_3)$_2$); 1.21 (12H, d, *J* = 6.3 Hz, CH(C*H*$_3$)$_2$) ppm.

^{t}Bu-DAB: ^{1}H NMR ($CDCl_3$)δ: 7.93 (2H, s, N=C*H*); 1.24 (18H, s, C(C*H*$_3$)$_3$) ppm.

*p*An-DAB: ^{1}H NMR ($CDCl_3$)δ: 8.49 (2H, s, N=C*H*); 7.39 (4H, d, *J* = 8.9 Hz, arom-H$_{(m\text{-OMe})}$); 6.97 (4H, d, *J* = 8.9 Hz, arom-H$_{(o\text{-OMe})}$); 3.86 (6H, s, OC*H*$_3$) ppm.

^{i}Pr-pyCa: ^{1}H NMR ($CDCl_3$)δ: 8.63 (1H, d, *J* = 5 Hz, py-H$_6$); 8.39 (1H, s, N=C*H*); 7.98 (1H, d, *J* = 8 Hz, py-H$_3$); 7.72 (1H, dd, *J* = 8/7 Hz, py-H$_4$); 7.29 (1H, dd, *J* = 7/5 Hz, py-H$_5$); 3.63 (1H, sept, *J* = 6.3 Hz, C*H*(CH_3)$_2$); 1.27 (6H, d, *J* = 6.3 Hz, CH(C*H*$_3$)$_2$) ppm.

Re(Me)(CO)$_3$(^{i}Pr-DAB): IR ν(CO) (THF)(cm^{-1}): 1995(vs); 1892 (s,br). UV–vis λ_{max}(ε in mol^{-1}cm^{-1})

(THF) (nm): 455(7150). ^{1}H NMR ($CDCl_3$)δ: 8.57 (2H, s, N=CH); 4.30 (2H, sept, J = 6.5 Hz, CH(CH_3)$_2$); 1.54/1.47 (6H/6H, d/d, J = 6.5 Hz, CH(CH_3)$_2$); −0.80 (3H, s, CH_3) ppm. MS(FAB$^+$): M(calc.), 425.511; M(exp.), 425.34.

Re(Et)(CO)$_3$(^{i}Pr-DAB): IR ν(CO) (THF)(cm^{-1}): 1994(vs); 1889 (s,br). UV–vis λ_{max} (ε in mol^{-1}cm^{-1})(THF)(nm): 460(7400). ^{1}H NMR ($CDCl_3$)δ: 8.56 (2H, s, N =CH); 4.35 (2H, sept. J = 6.5 Hz, CH(CH_3)$_2$); 1.71(3H, t, J = 7.8 Hz, CH_2CH_3); 1.51/1.49 (6H/6H, d/d, J = 6.5 Hz, CH(CH_3)$_2$); −0.26 (2H, q, J = 7.8 Hz, CH_2CH$_3$) ppm. MS (EI$^+$): M(calc.), 439.540; M(exp.) 439.41.

Re(Benz)(CO)$_3$(^{i}Pr-DAB): IR ν(CO) (THF)(cm^{-1}): 1998(vs); 1894 (s,br). UV–vis λ_{max} (ε in mol^{-1}cm^{-1}) (THF) (nm): 432(4950); 488(sh). ^{1}H NMR ($CDCl_3$)δ: 8.32 (2H, s, N=CH); 7.02 (2H, t, J = 7.6 Hz, arom-H); 6.74 (1H, t, J = 7.3 Hz, arom-H); 6.45 (2H, d, J = 7.0 Hz, arom-H); 4.06 (2H, sept, J = 6.5 Hz, CH(CH_3)$_2$); 1.77 (2H, s, CH_2=Ph); 1.50/1.24 (6H/6H, d/d, J = 6.5 Hz, CH(CH_3)$_2$) ppm. MS(EI$^+$): M(calc.), 501.613; M(exp.), 501.50.

Re(Me)(CO)$_3$(^{t}Bu-DAB): IR ν(CO) (THF)(cm^{-1}): 1994(vs); 1886 (s,br). UV–vis λ_{max} (ε in mol^{-1}cm^{-1}) (THF)(nm): 450(5150). ^{1}H NMR ($CDCl_3$)δ: 8.66 (2H, s, N=CH); 1.60 (18H, s, C(CH_3)$_3$); −0.83 (3H, s, CH_3) ppm. MS(FAB$^+$): M(calc.), 453.569; M(exp.), 453.67.

Re(Et)(CO)$_3$(^{t}Bu-DAB): IR ν(CO) (THF)(cm^{-1}): 1992(vs); 1884(s,br). UV–vis λ_{max} (ε in mol^{-1}cm^{-1}) (THF) (nm): 455(4800). ^{1}H NMR ($CDCl_3$)δ: 8.64 (2H, s, N=CH); 1.62 (3H, t, J = 7.5 Hz, CH_2CH_3); 1.61 (18H, s, C(CH_3)$_3$); −0.32 (2H, q, CH_2CH$_3$) ppm. MS(FAB$^+$): M(calc.), 467.597; M(exp.) 468.51 [1].

Re(Bz)(CO)$_3$(^{t}Bu-DAB): IR ν(CO) (THF)(cm^{-1}): 1998(vs); 1892 (s,br). UV–vis λ_{max} (THF)(nm): 434; 520(sh). ^{1}H NMR ($CDCl_3$)δ: 8.65 (2H, s, N=CH); 7.08 (2H, t, J = 7.0 Hz, arom-H); 6.83 (2H, d, J = 7.4 Hz, arom-H); 6.76 (1H, t, J = 7.2 Hz, arom-H); 1.63 (18H, S, C(CH_3)$_3$); 1.63 (2H, s, CH_2Ph) ppm. MS(FAB$^+$): M(calc.), 529.670; M(exp.), 530.6 [1].

Re(Me)(CO)$_3$(pAn-DAB): IR ν(CO) (THF)(cm^{-1}): 2000(vs); 1911(m); 1895(m). UV-vis λ_{max} (ε in mol^{-1} cm^{-1}) (THF)(nm): 403(12 700); 500(7000). ^{1}H NMR ($CDCl_3$)δ: 8.60 (2H, s, N=CH); 7.38 (4H, d, J = 8.7 Hz, arom-H$_{(m\text{-OMe})}$); 6.98 (4H, d, J = 8.7 Hz, arom-H$_{(o\text{-OMe})}$); 3.88 (6H, s, OCH_3); −0.55 (3H, s, CH_3) ppm. MS(FD$^+$): M(calc.), 553.600; M(exp.), 553.6.

Re(Me)(CO)$_3$(^{i}Pr-pyCa): IR ν(CO) (THF)(cm^{-1}): 1992(vs); 1882(br,s). UV–vis λ_{max} (ε in mol^{-1} cm^{-1}) (THF)(nm): 323; 445 (3980). ^{1}H NMR ($CDCl_3$)δ: 9.07 (1H, d, J = 5 Hz, py-H$_6$); 8.82 (1H, s, N=CH); 7.88 (2H, m, py-H$_3$/H$_4$); 7.36 (1H, dd, J = 5/5 Hz, py-H$_5$); 4.24 (1H, sept, J = 6.5 Hz, CH(CH_3)$_2$); 1.58/1.50 (2 × 3H, d, J = 6.5 Hz, CH(CH_3)$_2$); −0.94 (3H, s, CH_3) ppm. MS(FAB$^+$): M(calc.), 433.488; M(exp.), 434.2 [1].

Re(Et)(CO)$_3$(^{i}Pr-pyCa): IR ν(CO) (THF)(cm^{-1}): 1990 (vs); 1883 (br,s). UV–vis λ_{max} (ε in mol^{-1} cm^{-1}) (THF)(nm): 331; 457(4700). ^{1}H NMR ($CDCl_3$)δ: 9.06 (1H, d, J = 6 Hz, py-H$_6$); 8.84 (1H, s, N=CH); 7.86 (2H, m, py-H$_3$/H$_4$); 7.36 (1H, dd, J = 6.5/6 Hz, py-H$_5$); 4.26 (1H, sept, J = 6.6 Hz, CH(CH_3)$_2$); 1.58/1.51 (2 × 3H, d, J = 6.6 Hz, CH(CH_3)$_2$); 1.40 (3H, t, J = 7.8 Hz, CH_2CH_3); 0.12 (1H, dq, J = 7.8/11.1 Hz, CHHCH$_3$); −0.82 (1H, dq, J = 7.8/11.1 Hz, CHHCH$_3$) ppm. MS(FAB$^+$): M(calc.), 447.516; M(exp.), 448.06 [1].

2.3. Spectroscopic measurements

Preparations of samples for spectroscopic studies were carried out under purified N_2 by use of Schlenk techniques. The solutions were carefully handled in the dark before the experiments were performed.

Electronic absorption spectra were measured on a Varian Cary 4E spectrophotometer and a Perkin-Elmer Lambda 5 UV–vis spectrophotometer, provided with a 3600 Data Station. Infrared spectra were recorded on a Biorad FTS-7 or FTS-60A FT-IR spectrometer equipped with a liquid nitrogen-cooled MCT detector. The ^{1}H NMR spectra were recorded on a Bruker AMX 300 spectrometer.

Fast atom bombardment (FAB), field desorption (FD) and electron impact (EI) mass spectra were obtained with a JEOL JMS SX/SX102A four-sector mass spectrometer, coupled to a JEOL MS-MP7000 data system. For EI, the samples were introduced via the direct insertion probe into the ion source. For FAB, the samples were placed in a matrix solution (glycerol, thioglycerol, nitrobenzyl alcohol) onto a stainless probe and bombarded with xenon atoms with an energy of 3 keV. For FD, the sample was dissolved in methanol/water and then placed on the emitters by the dipping technique. An emitter current of 15 mA was used to desorb the sample. The ion source temperature was 363 K.

Resonance Raman measurements were performed on a Dilor XY spectrometer, using an SP model 2016 Ar ion laser as the excitation source. To avoid photodecomposition during the measurements, the KNO_3 pellet containing the complex was kept spinning and the exciting laser beam directed through a rotating prism. For measurements in solution a concentration of ca. 4×10^{-3} M was used and samples were contained in a spinning cell.

UV–photoelectron spectra were recorded on a Perkin-Elmer PS-18 photoelectron spectrometer, pro-

[1] Mass of M−H$^+$, due to proton abstraction of the matrix solvent in the mass spectrometer.

Table 1
Crystallographic data for Re(Me)(CO)$_3$(^{i}Pr-DAB)

Chemical formula	$C_{12}H_{19}O_3N_2Re$	V(Å^3)	3045.4(7)
Formula weight	425.5	D_{calc}(g cm^{-1})	1.86
Lattice type	tetragonal	F(0, 0, 0)	1632
Space group	$I4_1/a$	λ(Cu Kα) (Å)	1.5418
Z	8	μ(Cu Kα)(cm^{-1})	150.66
a(Å)	11.385(1)	T(K)	293
b(Å)	11.385(1)	R	0.060
c(Å)	23.495(3)	R_w	0.095

vided with a Helectros Developments hollow cathode He^I/He^{II} light source. The spectra were calibrated by use of He, Ar and Xe lines as internal references.

2.4. Crystal structure determination of Re(Me)(CO)$_3$(^{i}Pr-DAB)

The crystals were grown by slow evaporation of a THF solution. A crystal with approximate dimensions of 0.20 × 0.07 × 0.80 mm was used for data collection on an Enraf-Nonius CAD4 diffractometer with graphite-monochromated Cu Kα radiation and ω–2θ scan. A total of 1558 unique reflections was measured within the range $0 \le h \le 14$, $0 \le k \le 14$, $0 \le l \le 29$. Of these, 1505 were above the significance level of 2.5$\sigma(I)$. The maximum value of $(\sin\theta)/\lambda$ was 0.63 Å^{-1}. Two reference reflections ($\bar{2}20$, $\bar{4}02$) were measured hourly and showed no change during the 80 h collection time. Unit cell parameters were refined by a least-squares fitting procedure using 23 reflections with $80° < 2\theta < 87°$. Corrections for Lorentz and polarization effects were applied. The structure was solved by direct methods. The hydrogen atoms were placed in calculated portions.

Full-matrix least-squares refinement on F was carried out, anisotropic for the non-hydrogen atoms and isotropic for the hydrogen atoms, with the latter constrained so that the distance to the carrier remained constant at ca. 1.09 Å, and with the temperature factor of the hydrogen atoms fixed at $U = 0.038$ Å^2, and converged to $R = 0.060$, $R_w = 0.095$, $(\Delta/\sigma)_{max} = 0.21$. A weighing scheme $w = (13.2 + F_{obs} + 0.0037F_{obs}^2)^{-1}$ was used. An empirical absorption correction (DIFABS) [19] was applied, with coefficients in the range of 0.77–2.14. The secondary isotropic extinction coefficient [20,21] refined to $G = 0.10(2)$. A final difference Fourier map revealed a residual electron density between −1.2 and 1.7 e Å^{-3} in the vicinity of the Re atom. Scattering factors were taken from Cromer and Mann [22] and *International Tables for X-ray Crystallography* [23]. The anomalous scattering of the Re atom was taken into account. All calculations were performed with XTAL [23] unless stated otherwise.

The asymmetric unit contains half a molecule with the Re atom in a special position, giving rise to disorder in the molecule; half of the molecules in the crystal have the methyl on one side and the other half have it on the other side. So the atoms of the methyl group and the opposite carbonyl were refined with a occupancy factor of 0.5. Details of data collection, the unit cell and refinement parameters are summarized in Table 1.

Tables of anisotropic thermal parameter and hydrogen atom coordinates have been depended at the Cambridge Crystallographic Data Centre.

3. Results and discussion

3.1. Crystal structure of Re(Me)(CO)$_3$(^{i}Pr-DAB)

The molecular structure of Re(Me)(CO)$_3$(^{i}Pr-DAB) is presented as an ORTEP drawing in Fig. 2. The bond lengths and angles are listed in Table 2(a) and (b), respectively. Table 2(c) gives the final positional parameters and equivalent isotropic thermal parameters for the non-hydrogen atoms.

The structural data agree well with those for related complexes such as Re(Cl)(CO)$_3$(^{i}Pr-DAB) [24], Re(Cl)(CO)$_3$ (phen-pyCa) [25] and Mn(Br)(CO)$_3$(c-hex-DAB) [24]. The complex has a distorted octahedral geometry with C_s symmetry, the three carbonyls being coordinated in a *fac* geometry. The ^{i}Pr-DAB ligand has

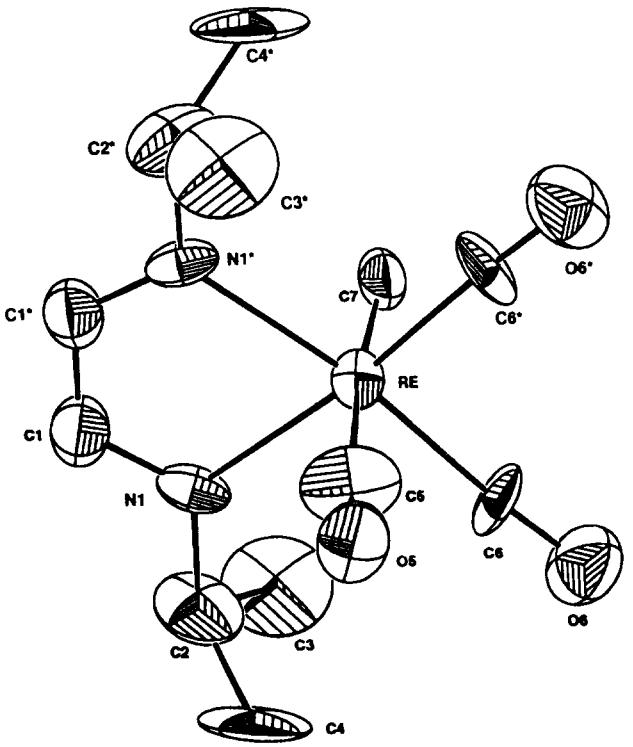

Fig. 2. Molecular structure (ORTEP drawing) for Re(Me)(CO)$_3$(^{i}Pr-DAB) with atom numbering.

a bite angle of 75.4°, and the axial methyl and carbonyl groups are bent slightly away from the ^{i}Pr-DAB ligand.

The bond lengths given in Table 2(a) for Re–C(5) and Re–C(7) are not very reliable. This is because the molecule lies on a twofold crystallographic rotation axis such that C(5) and C(7) atom sites almost exactly overlap due to the symmetry and as a consequence, their atom coordinates could not be refined independently. A quantitative assessment of the *trans*-effect of Me on the CO ligand was therefore not possible.

3.2. NMR spectroscopy

The ^{1}H NMR spectra of the Re(R)(CO)$_3$(α-diimine) compounds all show resonances for the imine proton in the δ 8.3–9.1 ppm region. These shifts indicate that the α-diimine ligands are coordinated in a σN–σN′ chelating manner [26–28].

The resonances of the alkyl groups were all found at low δ values, which means that the Re atom has a strong shielding effect. All the alkyl proton resonances show normal coupling patterns. However, the resonances of the α-hydrogens of the Et group in Re(Et)(CO)$_3$(^{i}Pr-pyCa) show an interesting feature (see Fig. 3) in that two separate signals were found, δ 0.62 and −0.47 ppm, respectively, both as a doublet of quartets. Thus, the two α-hydrogens are non-equivalent and couple with each other ($J_{H\alpha,H\alpha}$ = 11.1 Hz). The signals are split further by the β-hydrogens (J = 7.8 Hz).

This non-equivalence can be attributed to the asymmetry of the α-diimine ligand. This induces diastereotopic character in the β-hydrogen atoms. Raising the temperature did not change the coupling pattern for the Et group, not even not at a temperature of 383 K in toluene-d_8, in agreement with this explanation. This latter experiment also confirmed the high thermal stability of this compound, since only a small amount of the complex decomposed at this high temperature.

3.3. IR spectroscopy

The infrared spectra of all the Re(R)(CO)$_3$(α-diimine) complexes show two bands in the ν(CO) frequency region, the one at lower frequency being broad and consisting of two, nearly coincident, vibrations. These bands are assigned to the three IR-active CO stretching modes (2a′ + a″) of this type of complex having C_s symmetry [18,29,30].

Although the effects are small, the IR bands shift to lower frequency with a change in the α-diimine in the order *p*An-DAB > ^{i}Pr-DAB > ^{t}Bu-DAB > ^{i}Pr-PyCa. This trend is counted with the decrease in π-backbonding ability of the α-diimine. A similar effect was observed when the electron-withdrawing benzyl group was replaced by an electron-donating alkyl group such as methyl or ethyl.

3.4. UV–vis spectroscopy

The complexes were orange to red owing to the presence of an intense absorption band in the visible region between 400–500 nm. The extinction coefficients of these bands varied from 3980 mol^{-1} cm^{-1}

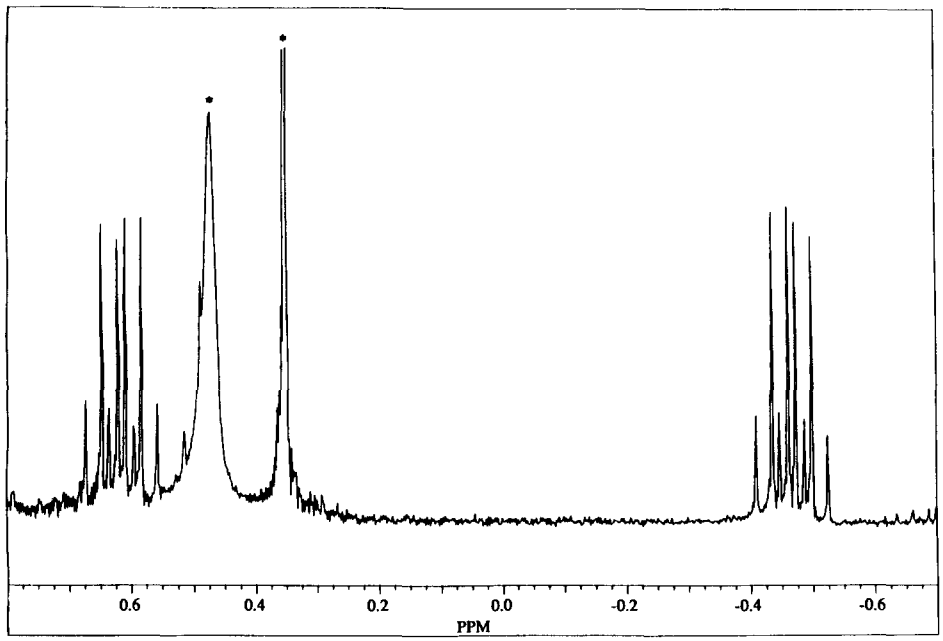

Fig. 3. The ReEt α-hydrogen region of the ^{1}H NMR spectrum of Re(Et)(CO)$_3$(^{i}Pr-pyCa) (benzene-d_6, 300 MHz) (* denotes contaminant in the solvent).

Table 2
(a) Bond distances (Å) in Re(Me)(CO)$_3$(^{i}Pr-DAB)

Atoms	Distance	Atoms	Distance
Re–C(5)	2.13(1)	C(2)–C(3)	1.50(2)
Re–C(6)	1.91(1)	C(2)–C(4)	1.54(2)
Re–C(6)*	1.91(1)	C(2)–N(1)	1.47(1)
Re–C(7)	1.89(4)	C(2)*–C(3)*	1.50(2)
Re–N(1)	2.177(8)	C(2)*–C(4)*	1.54(2)
Re–N(1)*	2.177(8)	C(2)*–N(1)*	1.47(1)
C(1)–C(1)*	1.41(2)	C(5)–O(5)	1.09(2)
C(1)–N(1)	1.28(1)	C(6)–O(6)	1.13(1)
C(1)*–N(1)*	1.28(1)	C(6)*–O(6)*	1.13(1)

(b) Bond angles (°) in Re(Me)(CO)$_3$(^{i}Pr-DAB) with standard deviations in parentheses

Atoms	Angle	Atoms	Angle
C(5)–Re–C(6)	86.9(9)	C(1)–C(1)*–N(1)*	119.1(9)
C(5)–Re–C(6)*	87.4(9)	C(3)–C(2)–C(4)	112(1)
C(5)–Re–C(7)	173(1)	C(3)–C(2)–N(1)	111(1)
C(5)–Re–N(1)	94.1(9)	C(4)–C(2)–N(1)	109(1)
C(5)–Re–N(1)*	92.1(9)	C(3)*–C(2)*–C(4)*	112(1)
C(6)–Re–C(6)*	88.5(4)	C(3)*–C(2)*–N(1)*	111(1)
C(6)–Re–C(7)	91.1(8)	C(4)*–C(2)*–N(1)*	109(1)
C(6)–Re–N(1)	98.1(4)	Re–C(5)b1O(5)	176(3)
C(6)–Re–N(1)*	173.3(4)	Re–C(6)–O(6)	177(1)
C(6)*–Re–C(7)	86.3(8)	Re–C(6)*–O(6)*	177(1)
C(6)*–Re–N(1)	173.3(4)	Re–N(1)–C(1)	113.1(6)
C(6)*–Re–N(1)*	98.1(4)	Re–N(1)–C(2)	128.3(7)
C(7)–Re–N(1)	92.3(8)	C(1)–N(1)–C(2)	118.3(9)
C(7)–Re–N(1)*	90.5(8)	Re–N(1)*–C(1)*	113.1(6)
N(1)–Re–N(1)*	75.4(3)	Re–N(1)*–C(2)*	128.3(7)
C(1)*–C(1)–N(1)	119.1(9)	C(1)–N(1)*–C(2)*	118.3(9)

(c) Fractional coordinates with standard deviations in parentheses and the equivalent isotropic thermal parameters for Re(Me)(CO)$_3$(^{i}Pr-DAB)

Atoms	x	y	z	U_{eq}
Re	0.5(0)	0.75(0)	0.34758(2)	0.0307(5)
C(1)	0.5178(9)	0.690(1)	0.2267(4)	0.049(5)
C(2)	0.568(1)	0.5136(9)	0.2735(6)	0.067(7)
C(3)	0.685(1)	0.500(1)	0.3012(8)	0.09(1)
C(4)	0.472(2)	0.4373(8)	0.3020(8)	0.09(1)
C(5)	0.318(1)	0.708(3)	0.354(1)	0.05(2)
C(6)	0.5253(9)	0.636(1)	0.4058(4)	0.052(6)
C(7)	0.659(4)	0.796(2)	0.3501(9)	0.05(2)
N(1)	0.5293(6)	0.6368(6)	0.2743(3)	0.035(4)
O(5)	0.226(1)	0.683(2)	0.3593(8)	0.07(1)
O(6)	0.5417(9)	0.5720(9)	0.4420(4)	0.072(6)

[Re(Me)(CO)$_3$(^{i}Pr-pyCa)] to 7400 mol^{-1} cm^{-1} [Re(Et)(CO)$_3$(^{i}Pr-DAB)]. The *p*An-DAB compound possessed an extra, strong, absorption band at 403 nm ($\varepsilon = 12\,700$), which arose from an intraligand $\pi \rightarrow \pi^*$ transition of the α-diimine ligand.

The lowest energy absorption band showed negative solvatochromism (see Table 3) which is characteristic for metal-to-ligand charge-transfer (MLCT) transitions, as has been shown for a series of α-diimine complexes such as M(CO)$_4$(α-diimine) (M = Cr, Mo, W) [1]. The solvatochromism decreased as the π-acceptor ability of the ligand increased (^{i}Pr-PyCa > ^{t}Bu-DAB > ^{i}Pr-DAB > *p*An-DAB). This can be attributed to an increased mixing between one of the dπ-orbitals of the Re atom and the π^*-orbital of the α-diimine ligand when they come close in energy. Through this increase in mixing or π-backbonding, the transition between these orbitals acquires more metal–ligand bonding to antibonding and less charge-transfer character. As a result, the solvatochromism becomes less pronounced.

Table 3
Absorption maxima [a] and their solvatochromism [b] for Re(Me)(CO)$_3$(α-diimine)

α-Diimine	CH_3CN	THF	Toluene	Δ [b]
^{i}Pr-pyCa	424	323, 445	338, 464	2033
^{t}Bu-DAB	434	450	465	1536
^{i}Pr-DAB	442	455	464	1073
*p*An-DAB	401, 489	403, 500	409, 508	765

[a] λ_{max} in nm.
[b] Difference in absorption maximum of the CT band in toluene and acetonitrile (in cm^{-1}).

The shift of the lowest-energy absorption band to lower energies on going from ^{i}Pr-pyCa to *p*An-DAB is caused by the lowering of the π^* level of the α-diimine ligand in this order.

Changing the alkyl group from Bz to Me to Et caused the MLCT band to shift to lower energy. This is due to an increase in energy of the dπ(Re)-orbitals as the alkyl group becomes more electron-releasing.

The UV–vis spectra of the Bz complexes were different from those of the Me and Et compounds (see Fig. 4). A distinct shoulder occurred on the low-energy side of the first absorption band and the extinction coefficient at the absorption maximum was much smaller than for the other complexes. Changing the solvent or lowering the temperature to 77 K had a similar effect on the shoulder and the band. Both features are therefore assigned to MLCT transitions. The dπ-orbitals of Re are probably considerably split by the interaction of the d_{xz}- and/or d_{yz}-orbitals with the π-orbitals of the benzyl group. This proposal is supported by the electrochemical data for the complexes [31]. The first oxida-

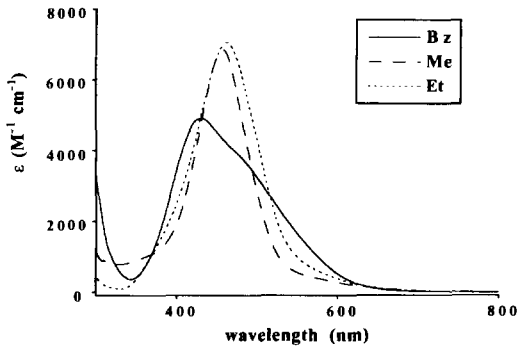

Fig. 4. Electronic absorption spectra of Re(R)(CO)$_3$(^{i}Pr-DAB) (R = Bz, Me, Et) in THF at room temperature.

tion potential of $Re(Bz)(CO)_3(^iPr\text{-}DAB)$ is found at +0.20 V (versus Fc/Fc^+ in ^nPrCN, RT), a much lower value than that for the corresponding Me or Et complex (+0.71 V for R = Me; +0.61 V for R = Et). This indicates that the highest-filled $d\pi$-orbital of the Bz complex is at a much higher energy. The higher electron-withdrawing ability of the benzyl group cannot account for this energy difference, since the maxima of the CT bands of the corresponding $Mn(R)(CO)_3(R'\text{-}DAB)$ complexes shifted to higher energy by only ca. 10 nm when Me was replaced by Bz [32].

3.5. Resonance Raman spectroscopy

In order to gain more insight into the character of the lowest-energy electronic transitions of the $Re(R)(CO)_3(\alpha\text{-diimine})$ complexes, resonance Raman (rR) experiments were carried out. Resonance Raman spectroscopy has proved to be very useful in characterizing allowed electronic transitions [12,33], since only those vibrations that are vibronically coupled to these transitions will be resonance-enhanced.

During the rR study, the wavelength of the exciting laser line was varied between 457.9 and 537.5 nm in order to obtain a quantitative picture of the rR effects in a so-called 'excitation profile' (EP). The high photoreactivity of most of the complexes [15] caused difficulties, and it was only possible to obtain reliable EPs for the $Re(Me)(CO)_3(R'\text{-}DAB)$ complexes, using a double spinning KNO_3 pellet. Only for the least photo-active complex, $Re(Me)(CO)_3(p\text{An-DAB})$, an EP could be obtained in benzene using a spinning cell.

Table 4 lists the most important Raman bands of the complexes and Fig. 5 depicts the Raman spectra of $Re(Me)(CO)_3(^tBu\text{-}DAB)$ at three different excitation wavelengths.

Table 4
Resonance-enhanced Raman bands for the complexes $Re(Me)(CO)_3(R\text{-}DAB)$ (R = ^{i}Pr, ^{t}Bu, *p*An) (KNO_3 disk, RT)

Ligand	Raman wavenumbers [a]
^{i}Pr-DAB	1988, 1511, 1359, 1156, 732, 503, 488, 451
^{t}Bu-DAB	1985, 1541, 1359, 1163, 1100, 768, 735, 649, 492, 484, 452
*p*An-DAB	1985, 1600, 1477, 1365, 1301, 1220, 1175, 1163, 1058, 868, 513, 470, 450

[a] In cm^{-1}.

The spectra can be considered in several sections and the assignments are based on a comparison with the spectra of, for example, $Re(X)(CO)_3(\alpha\text{-diimine})$ (X = halide) [33] and $Ph_3SnMn(CO)_3(\alpha\text{-diimine})$ [30]: (i) in the CO stretching frequency region there is one Raman band belonging to a $\nu_s(CO)$ vibration; (ii) in the frequency region of the ligand-stretching vibrations, a very strong Raman band shows up at ca. 1500 cm^{-1}, which is assigned to $\nu_s(CN)$ of the R'-DAB ligand [in addition, the $\nu_s(CC)$ band of the α-diimine skeleton (~1360 cm^{-1}) and the ν_s (C=C) band of the phenyl groups of *p*An-DAB (1600 cm^{-1}) appear in this region]; (iii) in the low-frequency region (800–200 cm^{-1}) there are many weak bands, some showing a weak rR effect. These bands cannot easily be assigned separately; they belong to $\nu_s(Re\text{–}N)$, $\delta(ReCO)$, $\nu_s(Re\text{–}CO)$ [34] and also to R'-DAB deformation modes.

The observation of rR effects for both $\nu_s(CN)$ and $\nu_s(CO)$ is in line with the MLCT character of these

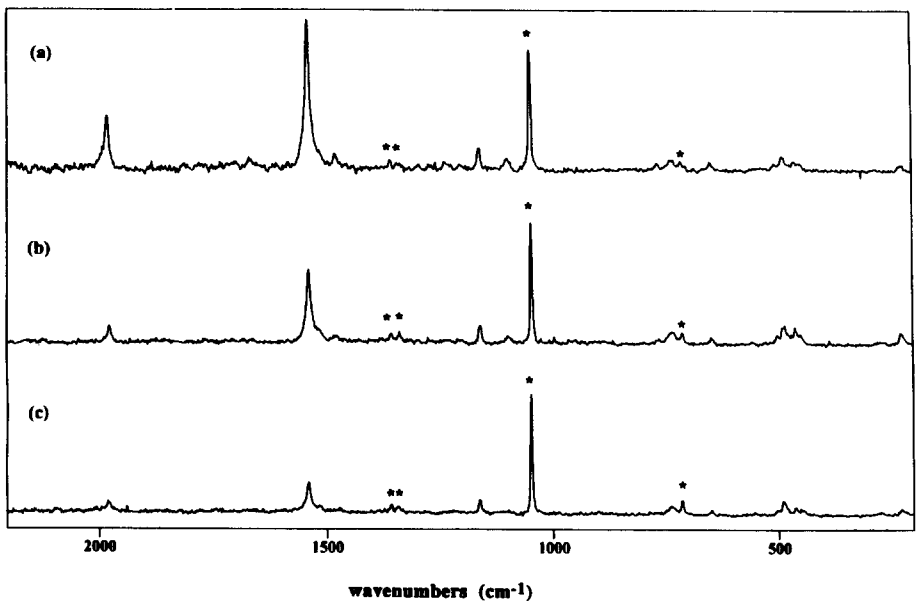

Fig. 5. Resonance Raman spectra of $Re(Me)(CO)_3(^tBu\text{-}DAB)$ in a KNO_3 disk at room temperature (a) λ_{exc} = 457.9 nm, (b) λ_{exc} = 514.5 nm and (c) λ_{exc} = 533.5 nm (* = KNO_3).

transitions. Depopulation of a metal $d\pi$-orbital decreases the metal-to-CO π-backbonding, and this in turn affects the CO distances and gives rise to the rR effect for ν_s(CO). Population of the lowest π^*-orbital of R′-DAB results in a weakening of the C=N bonds and this will give rise to the observed rR effect for ν_s(CN). The change in relative intensities of the ν_s(CO) and ν_s(CN) Raman bands throughout the absorption region (Fig. 6) is due to the presence of a second MLCT transition at higher energy. The maxima of these latter transitions could not be reached because of the restricted wavelength region of λ_{exc}(> 450 nm). Such transitions have, however, been observed for other α-diimine complexes such as M(CO)$_4$(α-diimine) [1], and they always give rise to a stronger rR effect for ν_s (CO) because of an increase in MLCT character with respect to the lower-energy transition.

The EP of Re(Me)(CO)$_3$(*p*An-DAB) showed a much stronger rR effect for ν_s(CN) upon excitation into the second, higher-energy band, which belongs to an IL transition. This strong effect is due to the large influence of a $\pi \rightarrow \pi^*$ (IL) transition on the CN bonds of the ligand compared with those of $d\pi \rightarrow \pi^*$ (MLCT) transitions. The IL transition also invoked rR effects for extra ligand modes at 1604, 1346 and 1077 cm^{-1}. Similar behaviour was found for Re(Cl)(CO)$_3$(*p*tol-DAB) [33].

The Raman spectra do not show a rR effect for ν(Re — Me), which is expected at ca. 450 cm^{-1} [34]. This means that the metal–methyl bond is not affected by the MLCT transitions. It also implies that the σ(Re — Me) $\rightarrow \pi^*$ (R′-DAB) transition does not contribute to the intensity of the first absorption band. This is not surprising since there would be hardly any overlap between σ(Re — Me) and π^*(R′-DAB). As a result, the photoreactions of these complexes, which will be discussed in a forthcoming article, can only take place from the $^3\sigma\pi^*$ state after surface crossing from a MLCT state, and not by direct irradiation into an allowed σ(Re — Me) $\rightarrow \pi^*$(R′-DAB) transition.

3.6. Ultraviolet–photoelectron spectra

In order to gain more information about the relative energies of the reactive $^3\sigma\pi^*$ state and the non-reactive $d\pi\pi^*$ (MLCT) states, a UV–photoelectron (UP) study was undertaken. Such UP spectra give the IPs of the various molecular orbitals by use of He^I/He^{II} excitation of a complex in the gas phase. Unfortunately, only in the case of the complex Re(Me)(CO)$_3$(^{i}Pr-DAB) was the thermal stability high enough and the vapour pressure sufficient to give reliable UP spectra. Andréa et al. [35], who studied the UP spectra of a series of M(X)(CO)$_3$(R-DAB) (M = Mn, Re; X = Cl, Br) complexes, likewise could only obtain the UP spectra for one of these complexes, viz. Re(Cl)(CO)$_3$(^{i}Pr-DAB). For Re(Me)(CO)$_3$(^{i}Pr-pyCa), a reliable UP spectrum could only be obtained by He^I excitation. The UP bands of this complex were assigned by comparison with those of Re(Me)(CO)$_3$(^{i}Pr-DAB).

The He^I and He^{II} UP spectra of Re(Me)(CO)$_3$(^{i}Pr-DAB) are shown in Fig. 7 and the IPs of the two Re(Me)(CO)$_3$(α-diimine) complexes are listed in Table 5 together with the data for related complexes.

The assignment of the UP bands is based on comparison with the data for the corresponding complexes M(CO)$_4$(^{i}Pr-DAB) (M = Cr, Mo, W) [35], Re(Cl)(CO)$_3$(^{i}Pr-DAB) [35] and (CO)$_5$ReRe(CO)$_3$(^{i}Pr-DAB) [11] and on the He^I/He^{II} intensity ratio differences [36–38]. In particular, for highly localized orbitals, qualitative arguments have proved to be very useful, and the following rules can be used to assign the spectra [39]: (i) metal d-type orbitals are characterized by strong enhancement of intensity upon going from He^I to He^{II} excitation; (ii) σ-orbitals have low He^{II} intensities because of the participation of s-orbitals; (iii) C and N 2p-type orbitals have comparable intensities in He^I and He^{II} which means that they normally lose intensity with respect to ionization from d-type orbitals on going from He^I to He^{II} excitation.

The d-orbitals of Re(Me)(CO)$_3$(^{i}Pr-DAB) have IPs

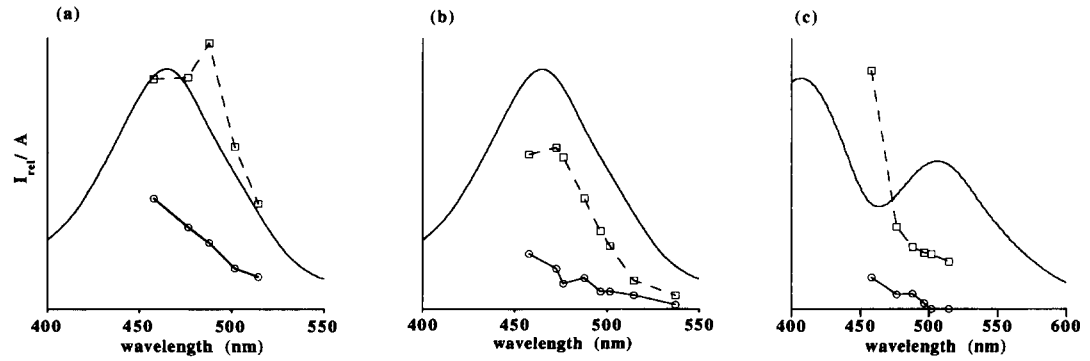

Fig. 6. Resonance Raman excitation profiles of ν_s(CO) (-○-○-○) and ν_s(CN) (--□--□--) of (a) Re(Me)(CO)$_3$(^{i}Pr-DAB) (b) Re(Me)(CO)$_3$(^{t}Bu-DAB) and (c) Re(Me)(CO)$_3$(*p*An-DAB); Intensities (I_{rel}) relative to the 1050 cm^{-1} band of KNO_3 for (a) and (b). For (c) I_{rel} relative to the 993 cm^{-1} band of benzene.

Table 5
Observed vertical ionization energies (eV) of $Re(Me)(CO)_3(^iPr\text{-}DAB)$ and $Re(Me)(CO)_3(^iPr\text{-}pyCa)$ together with literature data for $Re(Cl)(CO)_3(^iPr\text{-}DAB)$ and $(CO)_5Re'Re(CO)_3(^iPr\text{-}DAB)$

$Re(Me)(CO)_3(^iPr\text{-}DAB)$	$Re(Me)(CO)_3(^iPr\text{-}pyCa)$	$Re(Cl)(CO)_3(^iPr\text{-}DAB)$ [a]	$(CO)_5Re'Re(CO)_3(^iPr\text{-}DAB)$ [b]	Assignment
			7.03	σ(Re–Re')
7.23–7.79	7.10–7.62	7.76	7.54–8.00	d(Re)
8.50	8.26			σ(Re–Me)
			8.66–8.93	d(Re')
		9.59		Cl lone pair (e)
9.77			9.5	n_+(DAB)
		10.36		Cl lone pair (a_1)
11.06			10.99	n–π_2(–)(DAB)

[a] From Ref. [36].
[b] From Ref. [11].

of 7.23, 7.58 and 7.79 eV, so they are at higher energies than those of $Re(Cl)(CO)_3(^iPr\text{-}DAB)$. This difference in energy agrees with the shift of the MLCT band [456 nm for Me versus 442 nm for Cl [18] (in CH_2Cl_2)] and is caused by the stronger electron-donation by the alkyl group.

The complex $Re(Me)(CO)_3(^iPr\text{-}DAB)$ shows three other ionizations at 8.50, 9.77 and 11.06 eV. The last two are also present in the UP spectra of other ^iPr-DAB complexes, such as $M(CO)_4(^iPr\text{-}DAB)$ (M = Cr, Mo, W) [35] or $(CO)_5ReRe(CO)_3(^iPr\text{-}DAB)$ [11]. In the UP spectrum of $Re(Cl)(CO)_3(^iPr\text{-}DAB)$ these IPs partly overlap with Cl lone-pair ionizations. The IP at 9.77 eV varies between 9 and 10 eV for the other ^iPr-DAB complexes, and has been assigned to the n_+ lone-pair orbital of ^iPr-DAB. The 11.06 eV band has been assigned to ionizations from the π_2- and n_- orbitals of ^iPr-DAB.

The ionization at 8.50 eV is exceptional since it is not observed in the UP spectra of the above-mentioned

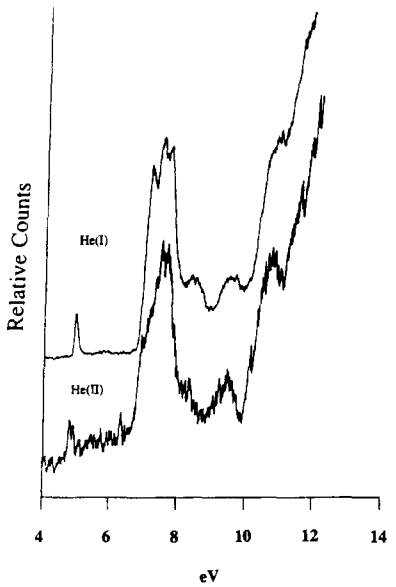

Fig. 7. He^I and He^{II} photoelectron spectra of $Re(Me)(CO)_3(^iPr\text{-}DAB)$.

^iPr-DAB complexes. It is assigned to the σ(Re — Me)-orbital, and this assignment agrees with the small cross-section of this ionization in the He spectra, which also excludes the possibility of a d-type orbital. This assignment is further supported by the ca. 1 : 3 intensity ratio of this ionization with respect to those from the d(Re)-orbitals.

The IPs of the σ(Re — Me)- and dπ(Re)-orbitals of $Re(Me)(CO)_3(^iPr\text{-}pyCa)$ are found at 8.26 and 7.10–7.62 eV, respectively. The slightly higher energies of the d(Re)-orbitals compared with those of the ^iPr-DAB complex can be attributed to stronger electron-donation by the ^iPr-pyCa ligand.

Comparing these results with the data obtained for the corresponding complexes $(CO)_5MM'(CO)_3(^iPr\text{-}DAB)$ (M, M' = Mn,Re) [11], which also possess a reactive $^3\sigma\pi^*$ state, we can conclude that the σ(Re — Me)- and σ(M — M')-orbitals are completely different in energy from the metal dπ-orbitals. In the metal–metal-bonded complexes, the σ-orbital is at higher energy, and in the metal–methyl complexes at a lower energy, than the d-orbitals. As a result, the reactive $^3\sigma\pi^*$ state of a metal–metal-bonded complex will be at lower energy than the MLCT states, which explains their high photoreactivity. The low photoreactivity of the $Re(Me)(CO)_3(\alpha\text{-diimine})$ complexes is then in accordance with the $^3\sigma\pi^*$ state being at higher energy than the MLCT states. Variation of the alkyl group is expected to influence the photoreactivity of these complexes owing to a change in relative energies of the $^3\sigma\pi^*$ and MLCT states. We have studied this effect and some preliminary results have been published [15].

4. Conclusion

The lowest-energy absorption bands of the complexes $Re(R)(CO)_3(\alpha\text{-diimine})$ are assigned to MLCT transitions with the aid of resonance Raman spectroscopy. The UV–photoelectron spectra show that in case of $Re(Me)(CO)_3(^iPr\text{-}DAB)$ the σ(Me — Re)-

orbital is lower in energy than the $d\pi$(Re)-orbitals, which implies that the MLCT states are lower in energy than the reactive $^3\sigma\pi^*$ state. This observation is of crucial importance for the interpretation of the photochemical behaviour of these complexes.

5. Supplementary material available

Listings of the bond distances (Table S1), bond angles (Table S2) and fractional coordinates, and isotropic thermal parameters (Table S3) for the hydrogen atoms. Listing of the anisotropic thermal parameters (Table S4). All available from the Cambridge Crystallographic Data Centre.

Acknowledgements

The Netherlands Foundation of Chemical Research (SON) and the Netherlands Organisation for the Advancement of Pure Research (NWO) are thanked for their financial support. A. Terpstra is thanked for recording the UV–photoelectron spectra.

References

[1] D.J. Stufkens, *Coord. Chem. Rev., 104* (1990) 39.
[2] D.J. Stufkens, T. van der Graaf, G.J. Stor and A. Oskam, *Coord. Chem. Rev., 111* (1991) 331.
[3] D.L. Morse and M.S. Wrighton, *J. Am. Chem. Soc., 98* (1976) 3931.
[4] J.C. Luong, R.A. Faltynek and M.S. Wrighton, *J. Am. Chem. Soc., 101* (1979) 1597.
[5] J.C. Luong, R.A. Faltynek and M.S. Wrighton, *J. Am. Chem. Soc., 102* (1980) 7892.
[6] D.J. Stufkens, *Comments Inorg. Chem., 13* (1992) 359.
[7] T.D. Westmoreland, K.S. Schanze, P.E. Neveux, Jr., E. Danielson, B.P. Sullivan, P. Chen and T.J. Meyer, *Inorg. Chem., 24* (1985) 2596.
[8] P. Chen, T.D. Westmoreland, E. Danielson, K.S. Schanze, D. Anthon, P.E. Neveux, Jr. and T.J. Meyer, *Inorg. Chem., 26* (1987) 1116.
[9] T.A. Perkins, W. Humer, T. Netzel and K.S. Schanze, *J. Phys. Chem., 94* (1990) 2229.
[10] K. Kaupp, H. Stoll, H. Preuss, W. Kaim, T. Stahl, G. van Koten, E. Wissing, W.J. Smeets and A.L. Spek, *J. Am. Chem. Soc., 113* (1991) 5606.
[11] R.R. Andréa, D.J. Stufkens and A. Oskam, *J. Organomet. Chem., 280* (1985) 63.
[12] H.A. Nieuwenhuis, D.J. Stufkens and A. Oskam, *Inorg. Chem., 33* (1994) 3212.
[13] H.A. Nieuwenhuis, A. Vlček, Jr. and D.J. Stufkens, *Inorg. Chem.*, submitted for publication.
[14] H.A. Nieuwenhuis, M.C.E. van de Ven, D.J. Stufkens, A. Oskam and K. Goubitz, *Organometallics, 14* (1995) 700.
[15] B.D. Rossenaar, C.J. Kleverlaan, D.J. Stufkens and A. Oskam, *J. Chem. Soc., Chem. Commun.*, (1994) 63.
[16] H. Bock and H. tom Dieck, *Chem. Ber., 100* (1967) 228.
[17] F.J. García Alonso, A. Llamazares, V. Riera, M. Vivanco, S. García Granda and M.R. Díaz, *Organometallics, 11* (1992) 2826.
[18] L.H. Staal, A. Oskam and K. Vrieze, *J. Organomet. Chem., 170* (1979) 235.
[19] N. Walker and D. Stuart, *Acta Crystallogr., A39* (1983) 158.
[20] W.H. Zachariasen, *Acta Crystallogr., A23* (1967) 558.
[21] A.C. Larson, in F.R. Ahmed, S.R. Hall and C.P. Huber (eds.), *The Inclusion of Secondary Extinction in Least-Squares Refinement of Crystal Structures. Crystallographic Computing*, Munksgaard, Copenhagen, ? pp. 291–294.
[22] D.T. Cromer and J.B. Mann, *Acta Crystallogr., A24* (1968) 321.
[23] S.R. Hall and J.M. Stewart (eds.), XTAL3.0 *User's Manual*, Universities of Western Australia and Maryland, 1990.
[24] A.J. Graham, B. Akrigg and B. Sheldrick, *Cryst. Struct. Commun., 6* (1977) 577.
[25] R.N. Dominey, B. Hauser, J. Hubbard and J. Dunham, *Inorg. Chem., 30* (1991) 4754.
[26] H. tom Dieck, I.W. Renk and K.D. Franz, *J. Organomet. Chem., 94* (1975) 417.
[27] G. van Koten and K. Vrieze, *Adv. Organomet. Chem., 21* (1982) 151.
[28] K. Vrieze, *J. Organomet. Chem., 300* (1986) 307.
[29] B.J. Brisdon, D.A. Edwards and J. White, *J. Organomet. Chem., 156* (1978) 427.
[30] R.R. Andréa, W.G.J. de Lange, D.J. Stufkens and A. Oskam, *Inorg. Chim. Acta, 149* (1988) 77.
[31] B.D. Rossenaar, F. Hartl and D.J. Stufkens, unpublished results.
[32] B.D. Rossenaar, D.J. Stufkens and A. Oskam, unpublished results.
[33] R.W. Balk, D.J. Stufkens and A. Oskam, *J. Chem. Soc., Dalton Trans.*, (1981) 1124.
[34] G.P. McQuillan, D.C. McKean, C. Long, A.R. Morrison and I. Torto, *J. Am. Chem. Soc., 108* (1986) 863.
[35] R.R. Andréa, J.N. Louwen, M.W. Kokkes, D.J. Stufkens and A. Oskam, *J. Organomet. Chem., 281* (1985) 273.
[36] A.H. Cowley, *Inorg. Chem., 26* (1979) 45.
[37] J.C. Green, *Struct. Bonding (Berlin), 43* (1981) 37.
[38] H. van Dam and A. Oskam, *Transition Met. Chem., 9* (1984) 125.
[39] A. Schweig and W. Thiel, *J. Phys. Chem., 60* (1974) 951.